Holocene eruptions of Mt. Popa, Myanmar: Volcanological evidence of the ongoing subduction of Indian Plate along Arakan Trench

A. Belousov [a,*], M. Belousova [a], Khin Zaw [b], M.J. Streck [c], I. Bindeman [d], S. Meffre [b], P. Vasconcelos [e]

[a] Institute of Volcanology and Seismology, Russia
[b] CODES, University of Tasmania, Hobart, Australia
[c] Portland State University, Portland, OR, USA
[d] University of Oregon, Eugene, OR, USA
[e] University of Queensland, Australia

ARTICLE INFO

ABSTRACT

In the western part of Myanmar the geodetic and seismic data indicate the ongoing highly oblique subduction of Indian Plate under Eurasian Plate. Volcanoes of Burma arc, however, did not produce eruptions in the recorded history and are considered extinct. Such perception questions the ongoing subduction, as well as keeping local officials unaware of possibility of future volcanic eruptions in the country. We have investigated the youngest lava flows and pyroclasts of Mt. Popa, which is the best-preserved polygenetic volcanic edifice in Myanmar. The Ar/Ar dating of the youngest products of the volcano provided very young radiometric ages which were unable to be measured accurately. The radiocarbon dating of paleosols intercalated with the most recent ash layers of the volcano has shown that Mt. Popa produced several eruptions in the beginning of Holocene. The youngest eruption occurred ~8000 BP and included the 1.3 km^3 gravitational collapse of the volcanic cone with deposition of the 11-km-long debris avalanche, immediately followed by emplacement of 0.1 km^3 of pyroclastic flow of calc-alkaline basaltic andesite composition. The collapse direction as well as complex morphology of the resulted crater were prearranged by geometry of the listric fault, which was formed during the pre-collapse asymmetric gravitational spreading of the volcanic cone. The recently erupted products are geochemically similar to products of young monogenetic volcanoes of Monywa area located 150 km north Mt. Popa, and both display patterns consistent with magma generation at an active subduction system. Low magma production rate of Mt. Popa (3×10^{-5} km^3/year averaged for the 1 Ma of the volcano history) is in agreement with the highly oblique angle and slow rate of the subduction. The fact of the Holocene eruptions of calc-alkaline composition in Burma arc represents volcanological evidence of the ongoing subduction in this part of the collision zone between India and Asia.

© 2018 Elsevier B.V. All rights reserved.

1. Introduction

The vast majority of active volcanoes of SE Asia are located along the 5000-km-long system of volcanic arcs jointly referred as Sunda Arc (Fig. 1). Volcanism of the arc is caused by the ongoing subduction of Indian and Australian Plates under Sunda Plate with rates up to 6–7 cm/year (DeMets et al., 1990; Tregoning et al., 1994). The volcanism is most intensive where the subduction is nearly orthogonal (e.g. in Java), and quickly fades out along the arc northward, where the angle of the plate convergence becomes increasingly oblique. The northernmost volcano of the arc previously known to be active is Barren Island in the Andaman Sea. Farther north there are no volcanoes with confirmed historical eruptions (the historical period in the area starts from approximately 1000 BP).

The modern tectonic regime of the northernmost part of Sunda arc (including Myanmar) has been debated for a long time (e.g. Stephenson and Reading, 1979; Curray, 1989; Bertrand and Rangin, 2003). Originally it was thought that relative motion of the Eurasian and Indian plates in this area is completely accommodated by several strike-slip dextral faults. Recent GPS measurements, however, indicate their highly oblique convergence on the Arakan (Rakhine) Trench. The subduction direction is oriented N35°E with a velocity of 23 mm/year, which is partitioned as 18 mm/year of right-lateral strike slip and 13 mm/year of convergence (Socquet et al., 2006). Local seismicity shows the Benioff Zone with average dip of 42° and penetration depth into the mantle up to 120–140 km (Satyabala, 1998, 2003; Dasgupta et al., 2003; Steckler et al., 2008; Hurukawa et al., 2012). Thus, the modern tectonic regime in the territory of Myanmar is suitable for

* Corresponding author.
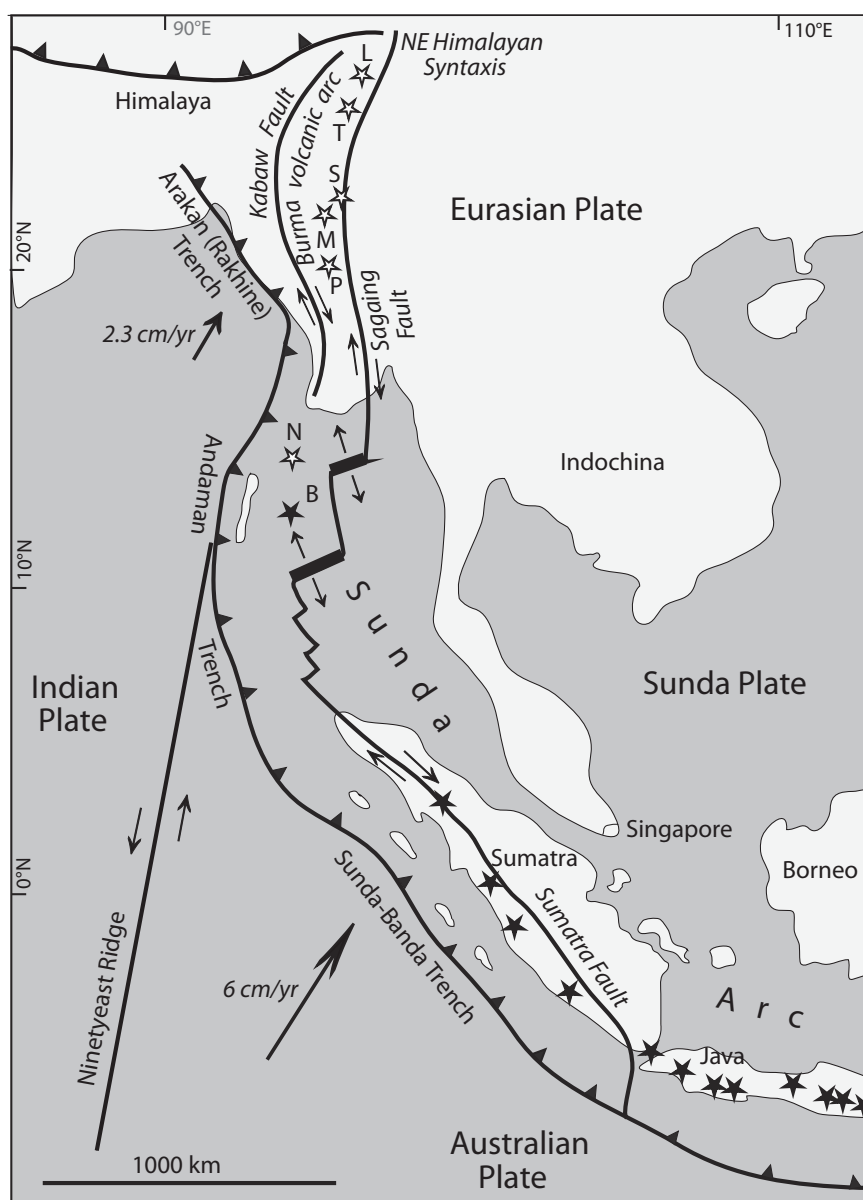E-mail address: belousov@mail.ru (A. Belousov).

Fig. 1. Structural sketch map of Sunda arc including the territory of Myanmar (with modifications after Sheth et al., 2009). Black stars indicate active volcanoes. White stars indicate volcanoes of the northern part of Sunda arc with no historical eruptions. Letters indicate the volcanoes Barren (B), Narcondam (N), Popa (P), Monywa (M), Singu (S), Taungthonlon (T), and Loimye (L). Arrows indicate the directions of tectonic motions.

generation of calc-alkaline magmas in the context of an active continental margin.

In Myanmar, there are several Pliocene-recent volcanic edifices that are widely scattered and line up to what is commonly referred as Burma volcanic arc, also known as Popa-Loimye, or Wuntho–Popa arc (Fig. 1). These edifices are represented by polygenetic composite cones of Mt. Popa, Taungthonlon, and Loimye, as well as monogenetic volcanoes of Monywa area (Chhibber, 1934). The calc-alkaline affinity of the erupted products indicates that magmas of these volcanoes could be explained by hydrous melting of a subduction-modified mantle (Maury et al., 2004; Mitchell et al., 2012). However Lee et al. (2016), basing on the geochemical heterogeneity of the erupted products, suggested that the oblique subduction of the Indian oceanic plate switched to dextral movement approximately 15 Ma ago and the Quaternary volcanism was connected to the subsequent "rollback" of the subducted lithosphere. Also, there is some controversy about the timing of when volcanoes of the Burma arc were last active. On one hand, some of the edifices have retained primary volcanic features suggesting Holocene age, but

the lack of confirmed historical eruptions and fumarolic activity of these volcanoes argue against that and in turn question whether subduction in this part of the plate boundary between India and Asia is ongoing.

The best-preserved volcanic landforms of Burma arc are Mt. Popa and monogenetic volcanoes of Monywa (Fig. 1). Chhibber (1934), referring to a local legend reported by Bell (1907), suggested that Mt. Popa could have had an eruption 442 BCE. In the Monywa area 150 km north of Mt. Popa, the youngest eruptions, probably of Holocene age, formed the NE trending chain of 5 maars, including Twin Taung and Twinywa (Chhibber, 1934; Bender, 1983; Maury et al., 2004). Around them, there are several older maars, scoria cones, and lava flows. Along with Mt. Popa, this area has the potential for future eruptions. We focused our investigation at Mt. Popa. The goal was to determine the timing and type of the most recent eruptions of this volcano, as well as to investigate the origin and age of a conspicuous volcaniclastic fan that came out from the crater breach. The fan deposit was described as lahar or debris flow by Stephenson and Marshall (1984), later
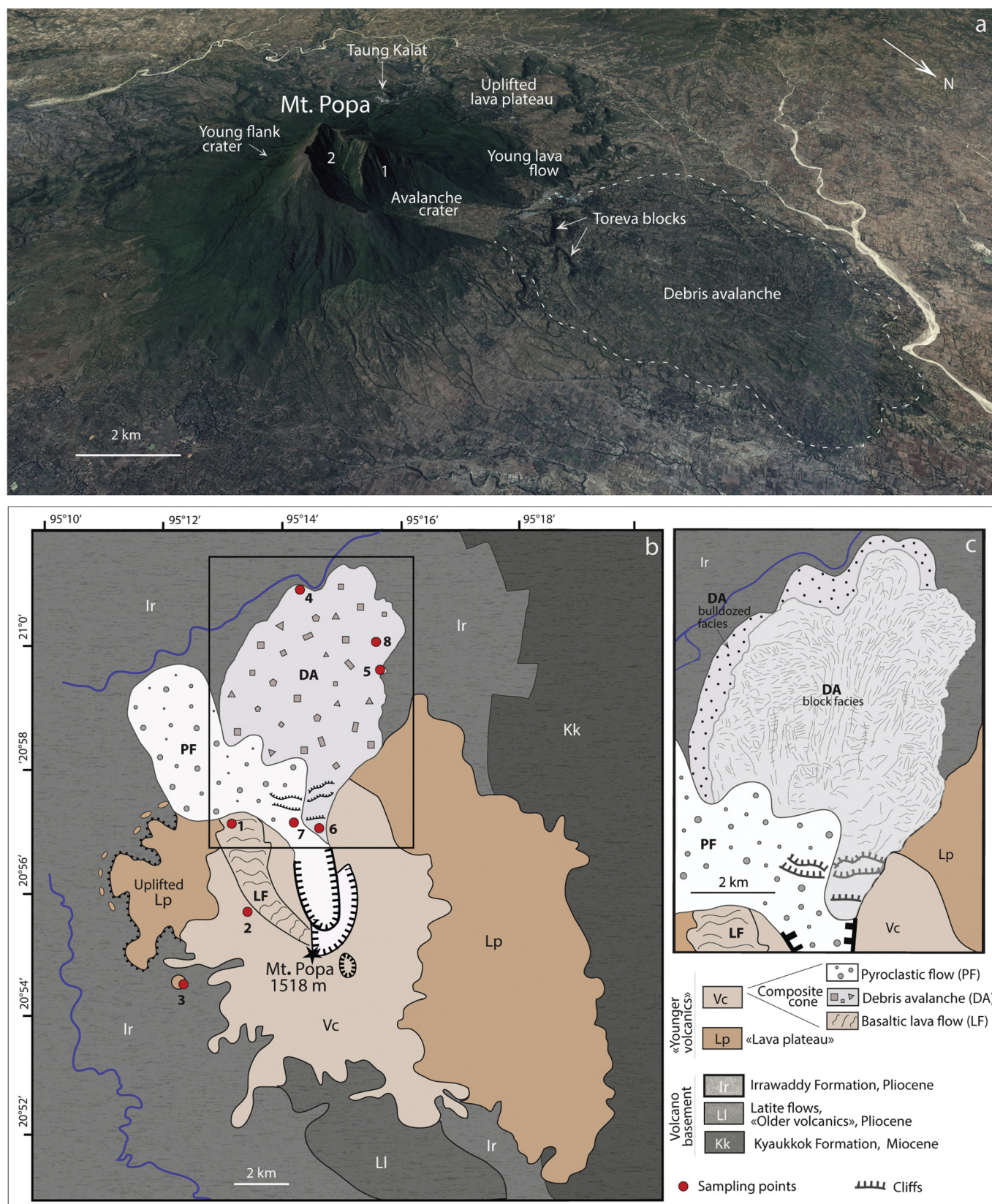
Fig. 2. (a) Perspective view of the edifice of Mt. Popa from NE with the main morphological features indicated, Google Earth image. The numbers indicate correspondingly the inner (1) and outer (2) "horseshoes" of the avalanche crater. (b) Geological sketch map of Mt. Popa area (with modifications after Stephenson and Marshall, 1984). Points with numbers indicate the outcrops and sampling locations described in the text. Rectangle outlines the area shown in c with more details. (c) Distribution of block facies and bulldozed facies as well as orientations of elongated hummocks on the surface of the 8000 BP debris avalanche deposit.

attributed to the sector collapse origin by Cumming et al. (2007). We compare the geochemistry of the recent products of Mt. Popa and monogenetic volcanoes of Monywa area with volcanic rocks of the nearby Andaman arc in order to shed more light on their geodynamic context.

2. Methodology

Our investigation of the structure and stratigraphy of volcanoes of Mt. Popa and Monywa was performed by geological field mapping in 2011 and 2012. Sampling of the erupted products was carried out in locations shown on Figs. 2b and 6a. In total, 25 samples of lava flows and volcaniclastic deposits were collected. Grain size analysis of samples of the volcaniclastic material was performed by standard dry sieving techniques (Walker, 1971). Surface morphology of pyroclastic particles was studied with scanning electron microscope JSM 6360 in Nanyang Technological University of Singapore. Details of methodology of isotope dating ($^{238}U/^{206}Pb$, $^{40}Ar/^{39}Ar$ and K/Ar dating) are shown in Table 1 and detailed in the electronic appendices. Radiocarbon dating of paleosol samples was performed by BETA Analytic Lab using the AMS (Accelerator Mass Spectrometer) method and calibration database INTCAL09 (Table 2). Whole rock major and trace element analyses by X-ray fluorescence (XRF) and inductively-coupled plasma mass spectrometry (ICP-MS) were carried out at the Geoanalytical Lab at Washington State University (WSU), Washington, USA following standard protocols of the Geoanalytical Lab; more details on analytical methods can be found in Streck et al. (2011).

3. Mt. Popa volcanic edifice

The steep-sided edifice of Mount Popa (1518 m asl) rises up to relative elevation of 1000 m over the rather flat area of the Central Burma Lowlands (Figs. 2 and 3a). This region structurally belongs to western part of the Salin subbasin that in turn belongs to the larger Central Basin of Myanmar (Pivnik et al., 1998). The volcanic cone is built on the junction of three older rock formations that are notably tectonically deformed (Fig. 2). The NNE-SE sector of the volcanic edifice rests on well-cemented arkose sandstones and shales of the Kyaukkok Formation (Upper Pegu group, Miocene), the SE-W sector rests on a massive latite lava flows forming a range of low hills south of Mt. Popa ("Older Volcanic group" of Chhibber, 1934; Pliocene in age), and the W-NNE sector covers weakly-cemented arkose sandstones and gravellites of the Irrawaddy (Ayeyarwady) Formation (Pliocene). These three formations are underlain by metamorphic basement as indicated by xenoliths of schist, slate, quartzite, and amphibolite found in the eruption products of Mt. Popa (Stephenson and Marshall, 1984; Pivnik et al., 1998). The edifice of Mt. Popa is a strongly truncated cone with a base diameter of 10 km. The volcano has large (3.5 × 2.5 km) deeply incised crater of complex morphology (Figs. 2 and 3a). In plan view, it can be geomorphically described as two nested horseshoes. The larger and broader outer horseshoe is about 2.7 km wide and has only one well-developed eastern branch. The smaller, inner horseshoe is about 1.3 km wide and 3 km long. The crater walls are up to 700 m high. The crater is breached to the north and a conspicuous broad fan composed of coarse volcaniclastic material emanates from this 1-km-wide breach (known as "Kyauktaga-Legyi agglomerate").

The volcano is composed of tectonically undeformed, calc-alkaline rocks ranging in composition from basalts to andesites (the "Younger volcanic group" of Chhibber, 1934; Maury et al., 2004; Mitchell et al., 2012, Lee et al., 2016). The lower part of the section of the "Younger volcanic group", emplaced by the initial eruptions of the volcano, forms a broad lava plateau (Fig. 2b). The lowest lava flows of the plateau have been dated at 0.81 to 1 Ma by Ar/Ar geochronology (Maury et al., 2004). The younger composite cone of Mt. Popa represents a complex assemblage of lava flows, dome material, and various volcaniclastic deposits (Chhibber, 1934; Stephenson and Marshall, 1984).

The W-NW base of the composite volcanic cone abuts on an uplifted sector of the lava plateau with dimensions 5 × 3 km. The uplifted sector is bounded by a steep outer cliff about 100 m high (Figs. 2 and 3c). The cliff is highly irregular in plan view with several radial dendritic valleys, each approximately 1 km long. Seven flat-topped elongated hills that form a broad arc along the outer cliff are erosional remnants of the original outer boundary of the uplifted sector. The morphologic features of both the volcanic edifice and the uplifted sector of the plateau resemble structures formed by gravitational asymmetric spreading (creep) of volcanic edifices (De Vries and Francis, 1997; Delcamp et al., 2008).

Near the western base of Mt. Popa, there is a prominent 100 m high rocky hill named Taung Kalat (or Taunggalla) that is a famous Buddhist landmark (Figs. 2a, b, and 3d). The hill is composed of poorly vesicular, slightly oxidized hornblende andesite lavas with coarse blocky joints. This geomorphic feature is commonly referred as a volcanic neck, however it does not contain classic features of volcanic conduits (e.g. vertical brecciated contacts with the wall rocks, signs of hydrothermal alteration etc.). Instead, it probably represents an erosional remnant of a lava flow (or several flows, because of the range in SiO_2 composition reported by Lee et al., 2016). The erosional remnant likely represents inverted topography as the lava flow(s) filled a paleo-depression that had developed in the weakly cemented Irrawaddy sandstone that was later eroded away. Our U-Pb zircon dating of the lava (location 3 in Table 1, Supplementary Table 1) gave an age 0.68 ± 0.04 Ma (disequilibrium and ^{207}Pb corrected $^{256}Pb/^{238}U$ laser ablation mass spectrometer age) indicating that it was emplaced by one of the earliest eruptions of Mt. Popa, or by one of its flank vents.

Table 1
Results of isotope dating of lavas and pyroclasts of volcanoes Mt. Popa and Monywa. Sampling locations see in Figs. 2b and 6a.

Location	Sample	Coordinates	Description of sample	Studied material	Method of dating	Age	Laboratory	Analyst	Details of dating
1 in Fig. 2b	Popa-Lava1	20°57′22.8″N 95°13′13.8″E	Lava flow, basalt	Hornblende	$^{40}Ar/^{39}Ar$	Zero (within limits of error)	University of Queensland	Thiede D., Vasconcelos P., Cohen B.	Supplementary Table 2
2 in Fig. 2b	Popa-PF1	20°55′49.5″N 5°13′22.5″E	Volcanic bomb, andesite	Hornblende	$^{40}Ar/^{39}Ar$	Zero (within limits of error)	University of Queensland	Thiede D., Vasconcelos P., Cohen B.	Supplementary Table 2
3 in Fig. 2b	Taung Kalat	20°54′46.9″N 95°12′10.5″E	Lava flow, basaltic andesite	Zircon	$^{238}U/^{206}Pb$	0.68 ± 0.04 Ma	University of Tasmania	Meffre S.	Supplementary Table 1
Mo-C2 in Fig. 6a	Cone2	22°17′56.3″N 95°2′3.7″E	Volcanic bomb, trachybasalt	Biotite	K/Ar	4.4 ± 0.5 Ma	CSIRO	Zwingmann H.	Supplementary Table 4
Mo-C3 in Fig. 6a	Cone3	22°22′0.10″N 95°1′48″E	Volcanic bomb, Twinywa maar, trachyandesite	Whole rock	$^{40}Ar/^{39}Ar$	85 ± 12 ka	University of Melbourne	Matchan E.	Supplementary Table 3
Mo-D3 in Fig. 6a	Dome3	22°13′47.5″N 94°56′51.1″E	Lava flow, basalt	Whole rock	$^{40}Ar/^{39}Ar$	880 ± 90 ka	University of Melbourne	Matchan E.	Supplementary Table 3

Table 2
Results of radiocarbon dating of paleosols intercalated with volcaniclastic deposits of Mt. Popa. Dated by BETA Analytic by the method of Accelerator Mass Spectrometry (AMS); calibration database INTCAL09. Sampling locations see in Fig. 2b.

Location	Sample	Coordinates	Description of sample	Conventional age, years BP	Calibrated age, years BP
4 in Fig. 2b	Age2012	21° 0′52.6″N 95°14′17.6″E	Red paleosol under debris avalanche	14,370 ± 70	17,660–17,220
5 in Fig. 2b	Age2011/1	20°59′38.34″N 95°15′58.9″E	Brown paleosol underlying paleosol Age2011/2	10,660 ± 50	12,820–12,650
5 in Fig. 2b	Age2011/2	20°59′38.34″N 95°15′58.9″E	Brown paleosol overlying paleosol Age2011/1	7700 ± 50	8590–8400
6 in Fig. 2b	Age2011/4	20°56′49.5″N 95°14′39.9″E	Lowermost part of brown soil overlying debris avalanche	2410 ± 40	2700–2340

4. Deposits of the youngest eruptions of Mt. Popa

4.1. Lava flow

The youngest lava flow (the "North-Western outer flow" of Chhibber, 1934) with well-preserved original surface morphology descends along the NNW slope of the volcano (Fig. 2). The block flow, made up of hornblende-augite basalt, has well-defined lateral levees, transverse pressure ridges (ogives) in the lava channel, and steep lobate flow front. The profile of the flow indicates high viscosity of the effusive lava. Source of the flow was located in the summit area of the volcano that was later removed in the process of gravitational lateral collapse of the volcanic cone (see section Debris avalanche deposit). The frontal part of the flow up to 1 km wide and 50 m thick covers the NE edge of the cliff of the uplifted sector of the lava plateau. Total length of the flow is approximately 5 km, and its volume can be estimated as

0.1 km^3. This flow covers older pyroclasts containing bread crust bombs represented by hornblende andesite. Ar/Ar dating of the flow and the pyroclasts (correspondingly locations 1 and 2 in Fig. 2b) yield no resolvable radiometric ages (Table 1, Supplementary Table 2) indicating that neither is older than a few tens of thousands years.

4.2. Fallout ash deposits

On the southern slope of the volcano at an elevation of approximately 1200 m asl there is a small elongated crater with dimensions of 550 × 270 m (Fig. 2). This flank crater was a source of poorly sorted weakly cemented fallout ash deposit mantling upper slopes of the southern part of the volcano. Good preservation of the crater and of the ash layer indicates their young, possibly Holocene age.

Several thin (from millimeters to a few cm) layers of medium to fine grained volcanic ash (Figs. 4a and 5) intercalated with layers of paleosol
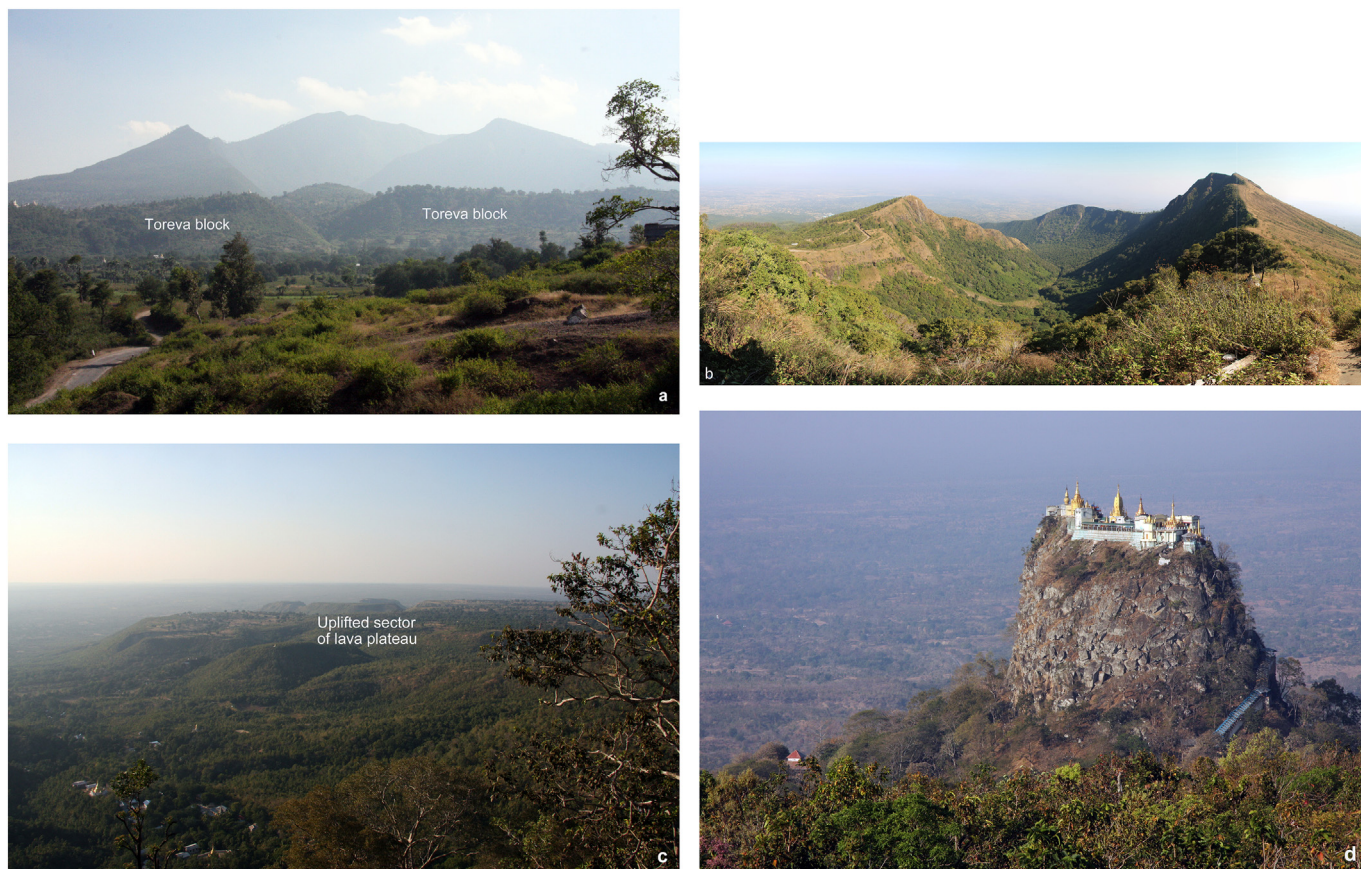
Fig. 3. Morphological features of Mt. Popa. (a) Mt. Popa from the N. Broad breach of the 8000 BP avalanche crater is visible behind the cliffs of the toreva blocks. Surface of the debris avalanche deposit in the foreground. (b) Avalanche crater of Mt. Popa as seen from its southern crater rim. (c) Uplifted sector of lava plateau at the western foot of Mt. Popa; view from the S from the top of the Taung Kalat hill. (d) Taung Kalat hill from SE. Photos by A. Belousov.

are buried under the debris avalanche deposit (see section The volcaniclastic fan) at location 5 at Fig. 2b. The ash clearly originated from some of the youngest eruptions of Popa - the only recent volcano in the area. Relatively poor sorting of the ash deposits with large percentage of fine-grained fraction as well as poor vesicularity and blocky shape of the ash particles indicate vulcanian character of these eruptions (Clarke et al., 2015). [14]C dating of the layer of paleosol separating the two youngest ash layers provided a calibrated age of 12,820–12,650 BP (Fig. 4a, Table 2). [14]C dating of the layer of paleosol, covering the youngest ash layer and separating it from the debris avalanche deposit
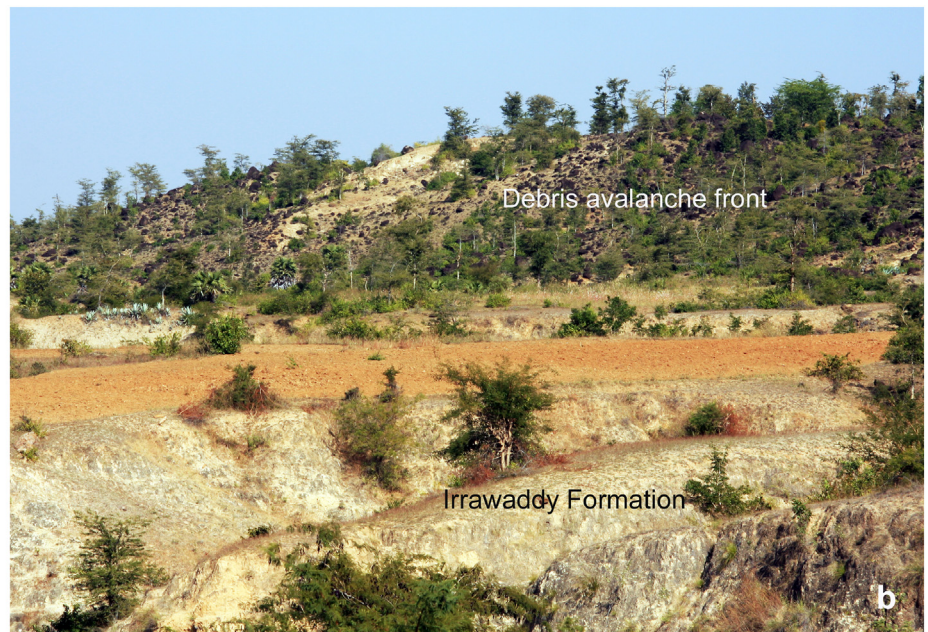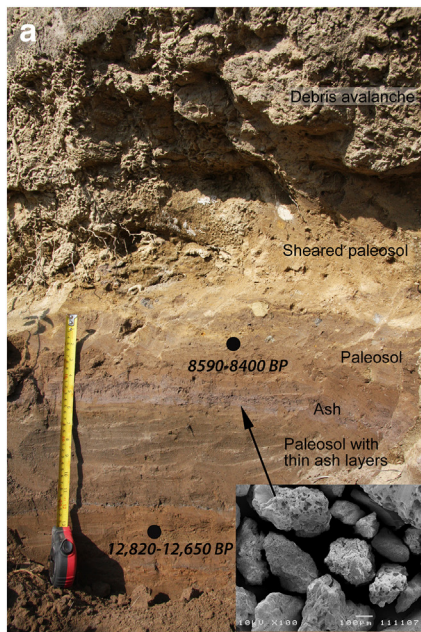
Fig. 4. Holocene volcaniclastic deposits of Mt. Popa. (a) Layers of volcanic ash in the paleosol buried by the 8000 BP debris avalanche deposit; location 5 in Fig. 2b. The inset shows scanning electron micrograph of particles from the uppermost ash layer. (b) Steep front of the debris avalanche deposit approximately 20 m high covering flat surface of sandstones of Irrawaddy formation. (c) Red laterite paleosol buried below the frontal part of the debris avalanche deposit comprised mostly of the bulldozed sandstones of Irrawaddy formation; location 4 in Fig. 2b. (d) Block facies of the debris avalanche deposit with fragmented, folded and faulted rocks of the collapsed volcanic cone; location 8 in Fig. 2b. (e) Pyroclastic flow deposit with the age ~8000 BP; location 7 in Fig. 2b. (f) Fossil fumarole in the pyroclastic flow deposit; location 7 in Fig. 2b. Photos by A. Belousov. Dots show sampling points of paleosol for radiocarbon dating and the obtained calibrated ages.
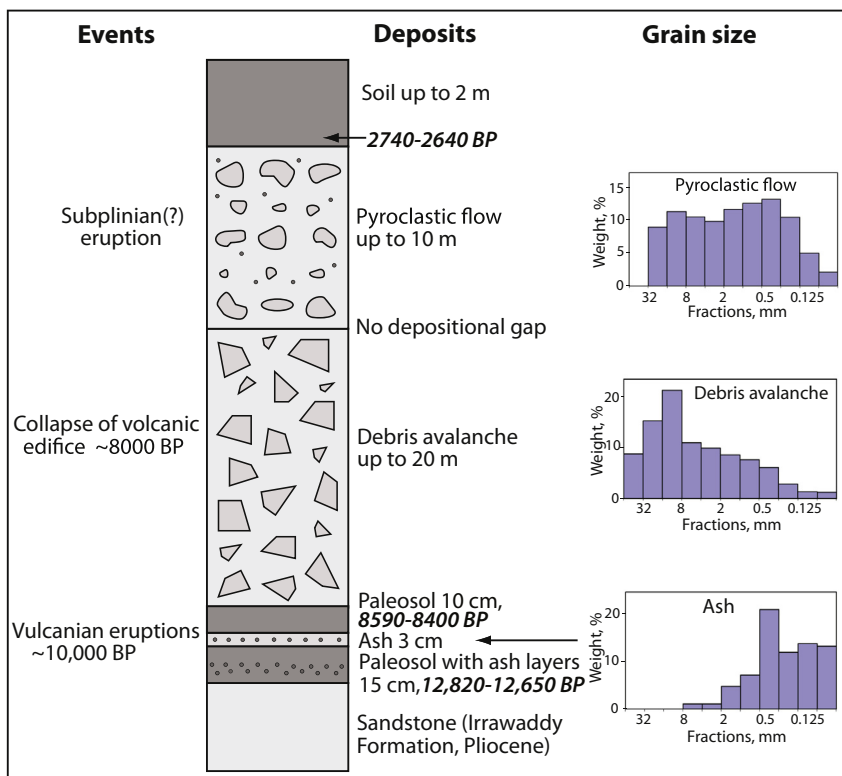

Fig. 5. Composite stratigraphic column and representative grain size histograms of the deposits of the volcaniclastic fan of Mt. Popa with suggested reconstruction of the eruptive events. Calibrated ^{14}C ages of paleosols are indicated.

above, provided a calibrated age of 8590–8400 BP. Thus, the deposition of this ash layers occurred at the very beginning of Holocene, shortly before the deposition of the debris avalanche. Some of these ashes could be produced by explosive activity associated with formation of the youngest lava flow and/or the flank crater of Mt. Popa.

4.3. The volcaniclastic fan

Investigation of the volcaniclastic fan (the "Kyauktaga-Legyi agglomerate") that came out of the crater breach revealed that it consists of two depositional units: a debris avalanche and a pyroclastic flow (Figs. 2 and 5).

4.3.1. Debris avalanche deposit

The debris avalanche deposit comprises a major part of the volcaniclastic fan. The lateral edges and the front of the deposit represent prominent escarpments that are 10–50 m high (Fig. 4b). The frontal part of the deposit is located at a distance of 11 km from the former summit of the volcano and 8 km from the crater breach. The deposit is approximately 5.5 km wide, 10–100 m thick (average thickness is about 50 m); and covers the area of 27 km^2. Its volume can be estimated as 1.3 km^3. The deposit has an undulating upper surface with gentle hummocks up to several tens of meters high. On and between the hummocks there are many scattered angular blocks of fragmented lava flow up to 3–5 m across. In plan view, many of the hummocks have elongated shapes; together they make for an intricate pattern of the avalanche flowage (Fig. 2c). Along the axis of the deposit area, the hummocks are strongly elongated and have mostly radial orientation (indicate extensional and shear deformations), while along its outer boundaries they are relatively short and have either chaotic or transverse orientations (indicate compressional deformations).

In the proximal area of the avalanche deposit (in the outlet of the crater breach) there are several large transverse hills with relatively gentle slopes facing the crater (southward), and much steeper slopes facing the distal part of the fan (northward) (Figs. 2 and 3a). The largest of the hills is 700 m × 300 m and 80 m high. These hills, originally described as Taungbaw and Ngayangon lava flows by Chhibber (1934), probably represent "toreva blocks" – the last portions of the collapsed edifice that did not transform into the debris avalanche and that came to rest close to the source (terminology after Reiche, 1937).

The internal structure of the debris avalanche deposit is poorly exposed. The few small quarries on its surface show that major volume of the deposit is comprised of typical block facies (terminology after Glicken, 1996). The avalanche blocks are irregular lenses of clastic material up to tens of meters across (Fig. 4c). The neighboring blocks differ in color, composition of the constituting rock clasts, and grain-size characteristics, and represent strongly deformed (stretched, folded, and faulted) layers of various pyroclastic material (tephra, block and ash flows etc.) that composed the collapsed volcanic edifice. Few of the avalanche blocks represent former lava flows and domes that were intensively brecciated in the process of the gravitational collapse. Rock clasts in the avalanche blocks are angular; many of them are fractured and show jigsaw puzzle features (Glicken, 1996). The deposit is poorly sorted (Fig. 5). The toreva blocks are composed of dense lava that experienced only incipient fracturing in the process of sliding.

Along the outer boundary of the avalanche, in a band up to several hundred meters wide, the deposit is composed of the material of block facies intermixed with the material of the avalanche substrate represented by fragmented sandstones of the Irrawaddy Formation (Fig. 2c). This is the "bulldozed facies" of the debris avalanche deposit (terminology after Belousov et al., 1999). The proportion of the entrained substrate material increases towards the outer boundary of the deposit, and its outer rim several tens meters wide in many locations consists completely of the sands and gravels of disintegrated Irrawaddy Formation. The bulldozed sands and gravels are thoroughly intermixed, structureless and contain sand concretions and large

fragments of silicified wood picked up from the Irrawaddy Formation. The bulldozed facies in several locations are thrusted on a layer of paleosol (Fig. 4c). The uppermost layer of the underlying paleosol along the contact with the bulldozed facies is sheared on a thickness 5–10 cm (Fig. 4a).

4.3.2. Age of the debris avalanche

No organic material suitable for ^{14}C dating was found inside the avalanche deposit. To estimate the age of the collapse we obtained the ^{14}C ages of the paleosols underlying the avalanche deposit (its bulldozed facies), and the paleosol overlying the avalanche (Table 2). At location 4 at Fig. 2b, the front of the debris avalanche deposit covered red laterite paleosol, the uppermost part of which provided a calibrated age of 17,660–17,220 BP (Fig. 4d). At location 5 at Fig. 2b, the debris avalanche deposit covered the sequence of ash layers intercalated with brown paleosols, the uppermost of which provided the calibrated age of 8590–8400 BP (Fig. 4a; see more details in section Fallout ash deposits). The lowermost part of brown soil overlying the debris avalanche deposit at location 7 at Fig. 2b provided a calibrated age of 2740–2640 BP. Thus, deposition of the debris avalanche occurred in time interval between 8590–8400 BP and 2740–2640 BP. It is well established that the age of emplacement of a volcaniclastic deposit is commonly close to the ^{14}C age of the buried paleosol, while the ^{14}C dating of the overlying paleosol provides much younger age (e.g. Scharpenseel and Schiffmann, 1977; Wang et al., 1996; Cherkinsky and Wallace, 2017). Consequently, the flank collapse that gave rise to the debris avalanche occurred close to the age of the underlying paleosol - approximately 8000 BP.

4.3.3. Pyroclastic flow

Along the western edge of the debris avalanche deposit and partly on top of it rests a scoriaceous pyroclastic flow deposit (Fig. 4e) originally described as "Later ashes, with bombs" by Chhibber (1934). The deposit has a well-preserved original gently inclined and planar upper surface. The lateral edges and front of the deposit are not expressed in the modern topography. The highly mobile flow filled depressions and leveled the paleorelief. Excellent outcrops of the deposit are located in the outermost part of the crater breach in several large quarries of the pozzolan factory (location 7 at Fig. 2b), as well as along the stream channel that drains the NW part of the crater. The deposit is friable, slightly compacted, matrix supported. The matrix is poorly sorted (Fig. 5). Clasts of dark grey scoriaceous basaltic andesite up to 1 m are evenly distributed throughout the flow thickness. Many clasts have cauliflower-shaped outer surfaces. Several fossil fumaroles (Fig. 4f) and abundant thin degassing pipes found in the deposit indicate that it was hot and gas-rich during deposition. The maximum thickness of the pyroclastic flow is 15 m. The deposit was traced up to a distance of 7 km from the volcano summit; it covers at least 5 km^2, and has approximately 0.1 km^3 volume. It was emplaced by the subplinian eruption of VEI 3 scale (Newhall and Self, 1982).

No charcoal suitable for radiocarbon dating was found in the pyroclastic flow deposit, but it rests directly on top of the debris avalanche deposit without signs of the depositional gap (no soil horizons or reworked material in-between). The lack of charcoal also supports the short depositional gap, indicating that vegetation had not yet recolonized the avalanche surface before the PF emplacement. Probably emplacement of the pyroclastic flow immediately followed the emplacement of the debris avalanche, and they both have essentially the same age (approximately 8000 BP).

5. Geochemistry of the youngest erupted magma

We analyzed the youngest erupted product of Mt. Popa (sample Po-PF2 in Table 3), a scoriaceous cauliflower bomb from the pyroclastic flow covering the debris avalanche deposit at location 7 at Fig. 2b. This sample is compared to one older sample from the composite cone of

Mt. Popa and to six samples from Pliocene-recent eruptions of Monywa area. The sample Po-DA4 (Table 3) was collected from large angular rock clasts on the surface of the debris avalanche deposit of Mt. Popa at location 8 at Fig. 2b. It represents a fragment of lava flow, the age and original stratigraphic position of which inside the volcanic cone is unknown.

Samples from Monywa area were taken from monogenetic volcanic edifices of two types (Fig. 6, Table 3). Samples Mo-D1 and Mo-D3 were collected from two well preserved lava flows (Fig. 6b). These lava flows were deposited over flat terrain and spread out as stubby circular flows 0.5–2 km in diameter, 20–50 m thick with volumes estimated as 0.05 km³ each. Ar/Ar age of the D3 flow is 880 ± 90 ka (Table 1, Supplementary Table 3). Samples Mo-C2, Mo-C3, Mo-C4, and Mo-C5 represent cauliflower bombs from wavy laminated base surge deposits of phreatomagmatic eruptions (Fig. 6c). Sample Mo-C2 from the base surge deposit exposed in the left bank of Chindwin River (the right tributary of Irrawaddy River) has K/Ar age of 4.4 ± 0.5 MA (Table 1, Supplementary Table 4). Other samples are from edifices of maars with well-preserved craters filled with modern lakes. These maars were formed probably in Late Pleistocene–Early Holocene. Sample Mo-C3 from Twinywa maar has Ar/Ar age of 85 ± 12 ka (Fig. 6a, c and d; Table 1, Supplementary Table 3).

Samples from Popa and Monywa range in composition from subalkaline basalt to andesite (Fig. 7a; Table 3). Two samples (Mo-C2 and Mo-C3) straddle the boundary to trachybasalt and to trachyandesite, respectively. With regards to K_2O, the samples range from medium K (calc-alkaline) to high K to shoshonitic. On mantle normalized incompatible trace element diagrams, the samples from both areas display patterns that are consistent with magma generation at an active subduction system with strong relative depletion of Nb, Ta,

Zr, Hf in all samples and mild relative enrichment in Sr and Pb of some samples (Fig. 7b). In comparison to their oceanic counterpart, Barren Island, basaltic samples are considerably more enriched in the most incompatible trace elements with the exception of Rb that is equally low leading to a distinct relative depletion of Rb to neighboring elements (Fig. 7b). A noteworthy difference of all Monywa and Popa samples relative to Barren Island and Narcondam is their strong Zr and Hf troughs.

6. Discussion

The new data presented in this study on the geology of Mt. Popa and Monywa, combined with data from previous research, can be summarized as follows.

6.1. Geological history of Mt. Popa

The edifice of the volcano started to form approximately 1 Ma ago (Maury et al., 2004). The first products of the volcano were deposited on folded rocks of Miocene and Pliocene age leveled by erosion. Throughout its history the volcano produced eruptions mostly of low to mild magnitudes and of diverse styles (both explosive and effusive: Chhibber, 1934; Stephenson and Marshall, 1984). By the beginning of the Holocene this activity formed composite volcanic cone approximately 1200 m above the surrounding terrain and of 30 km³ in volume (the reconstruction is based on the present-day truncated cone and the shape of a regular cone). Thus, average rate of magma production of Popa volcano during 1 million years of activity comprised approximately 3×10^{-5} km³/year. This is two orders of magnitude lower than the rate typical for subduction-related volcanoes (Wadge, 1984; Crisp, 1984).

Table 3
Major and trace-element data on the recent volcanic products of Mt. Popa (samples with indexes *Po*) and Monywa (samples with indexes *Mo*). Sampling locations see in Figs. 2b and 6a.

	Po-DA4	Po-PF2	Mo-D1	Mo-C2	Mo-C3	Mo-D3	Mo-C4	Mo-C5
Coordinates	20°59′46.3″N	20°57′11.9″N	22°14′51.8″N	22°17′56.3″N	22°22′0.1″N	22°13′47.5″N	22°13′41.8″N	22°15′36.9″N
	95°15′41.8″E	95°14′19.4″E	95°05′25.2″E	95°2′3.7″E	95°1′48″E	94°56′51.1″E	94°59′57.5″E	94°57′0″E
XRF								
Normalized major elements (wt%)								
SiO_2	50,08	53,23	48,05	48,48	58,27	48,52	47,37	48,33
TiO_2	0,890	0,730	0,879	0,845	0,529	0,999	0,980	0,856
Al_2O_3	18,92	15,81	16,21	18,31	17,80	16,44	16,66	16,56
FeO*	8,95	7,50	8,93	9,56	5,47	9,04	8,99	8,86
MnO	0,148	0,130	0,173	0,181	0,124	0,178	0,166	0,172
MgO	5,59	7,81	11,38	4,69	3,35	8,88	9,49	10,04
CaO	11,02	11,12	11,10	12,49	8,04	11,81	13,27	11,49
Na_2O	2,93	2,40	2,39	2,77	3,90	2,91	2,21	2,80
K_2O	1,25	1,10	0,72	2,17	2,28	0,95	0,63	0,72
P_2O_5	0,223	0,179	0,161	0,499	0,233	0,273	0,241	0,166
Total	100,00	100,00	100,00	100,00	100,00	100,00	100,00	100,00
Unnormalized trace elements (ppm)								
Ni	23	42	181	11	18	126	94	144
Cr	19	230	462	7	40	288	294	366
Sc	28	32	35	17	15	34	39	35
V	266	220	262	279	149	255	299	259
Ba	464	459	400	1120	1530	633	692	438
Rb	15	19	14	42	59	16	14	19
Sr	873	798	575	2233	1192	833	848	603
Zr	81	70	73	139	143	92	84	79
Y	20	15	21	30	19	24	24	23
Nb	3,9	3,8	3,1	5,5	4,1	6,5	3,3	2,8
Ga	19	17	17	21	19	18	16	17
Cu	30	105	73	71	60	80	77	54
Zn	65	60	74	89	49	84	71	76
Pb	3	3	5	7	3	7	7	4
La	28	22	21	129	67	33	36	21
Ce	53	43	36	245	117	70	69	35
Th	6	6	4	24	19	10	8	3
Nd	28	23	19	109	46	30	28	19
U	1	2	1	7	5	2	2	2

Fig. 6. Monogenetic volcanoes of Monywa area. (a) Locations of the sampling points superimposed over the Google Earth image. (b) Quarry exposing internal part of a lava flow; sampling location D1. (c) Cross-laminated base surge deposits with bomb sags of phreatomagmatic eruption that formed maar Twinywa; sampling location C3 with Ar/Ar age of 85 ± 12 ka. (d) Maar Twinywa; diameter of the crater 1.6 km.
Photos b, c, and d by A. Belousov.

When the cone grew large enough, simultaneously with the eruptive activity, the process of its slow gravitational spreading started (Fig. 8). It was facilitated by the presence of easily deformable sedimentary rocks in the base of the volcano similar to other volcanoes worldwide (De Vries and Francis, 1997; Delcamp et al., 2008). The spreading was notably asymmetric; the W-NE sector creeped down faster because it rested on poorly lithified sandstones of Irrawaddy Formation. The other sectors were relatively stable because they rested over mechanically competent rocks. The southern sector, buttressed by a range of hills composed of latite lavas of "Older volcanic group", was the most stable. The preferential spreading towards W-NW formed an arcuate listric fault (possibly a set of listric faults) inside the cone. The detachment plane of the fault penetrated into the volcano base (into the sandstones of Irrawaddy Formation) and then went out to the ground surface at a distance 3 km from the foot of the volcanic cone, so the listric fault had "ramp-flat-ramp" geometry (Boyer and Elliott, 1982). Slow gravitational creep along this fault thrusted upward the W-NW sector of the lava plateau (Fig. 8). Similar asymmetric spreading occurred for example at several volcanoes in the Eastern Carpathians (Szakács and Krézsek, 2006).

At the end of Pleistocene to the beginning of Holocene (Fig. 5 and Table 2), the volcano was active and produced several explosive (of vulcanian type) and effusive eruptions of small to moderate scale; the youngest lava flow with the volume of 0.1 km^3 covered the NE part of the uplifted sector of the lava plateau. The last eruption of Mt. Popa

occurred about 8000 years ago. In the process of the magma ascent, which preceded the eruption, the volcanic edifice lost gravitational stability, and ~1.3 km^3 of the edifice (approximately 5% of its volume) slid down. The complex geometry of the resulted collapse crater can be explained by the retrogressive failure that involved the zones of mechanical weakness, which were formed inside the volcanic cone by the preceding gravitational spreading. The failure occurred in at least two stages (Fig. 8). The first major stage of the collapse (~1 km^3) formed the inner horseshoe-shaped depression of the crater, its direction coincided with direction of right lateral transfer fault of the arcuate listric fault. Then, probably immediately, followed the second stage of the collapse (~0.3 km^3) that enlarged the inner depression and formed the eastern branch of the outer horseshoe of the crater; its position and size was set by the head ramp of the arcuate listric fault.

The debris avalanche resulted from the gravitational collapse travelled 11 km from the source (Fig. 2). If the ratio of the height to travel distance (H/L) of the avalanche assumed to be 0.1, which is average for volcanic debris avalanches worldwide (Siebert, 1984), the pre-collapse relative elevation of the volcano can be calculated as 1100 m. This elevation is in good agreement with our reconstruction of 1200 m based on the present day cone morphology.

No deposit of directed blast associated with the collapse was found. Thus, as was shown by Belousov et al. (2007), in the moment of the gravitational failure the rising magma batch was situated deeper than the detachment plane of the collapse (there was no cryptodome inside
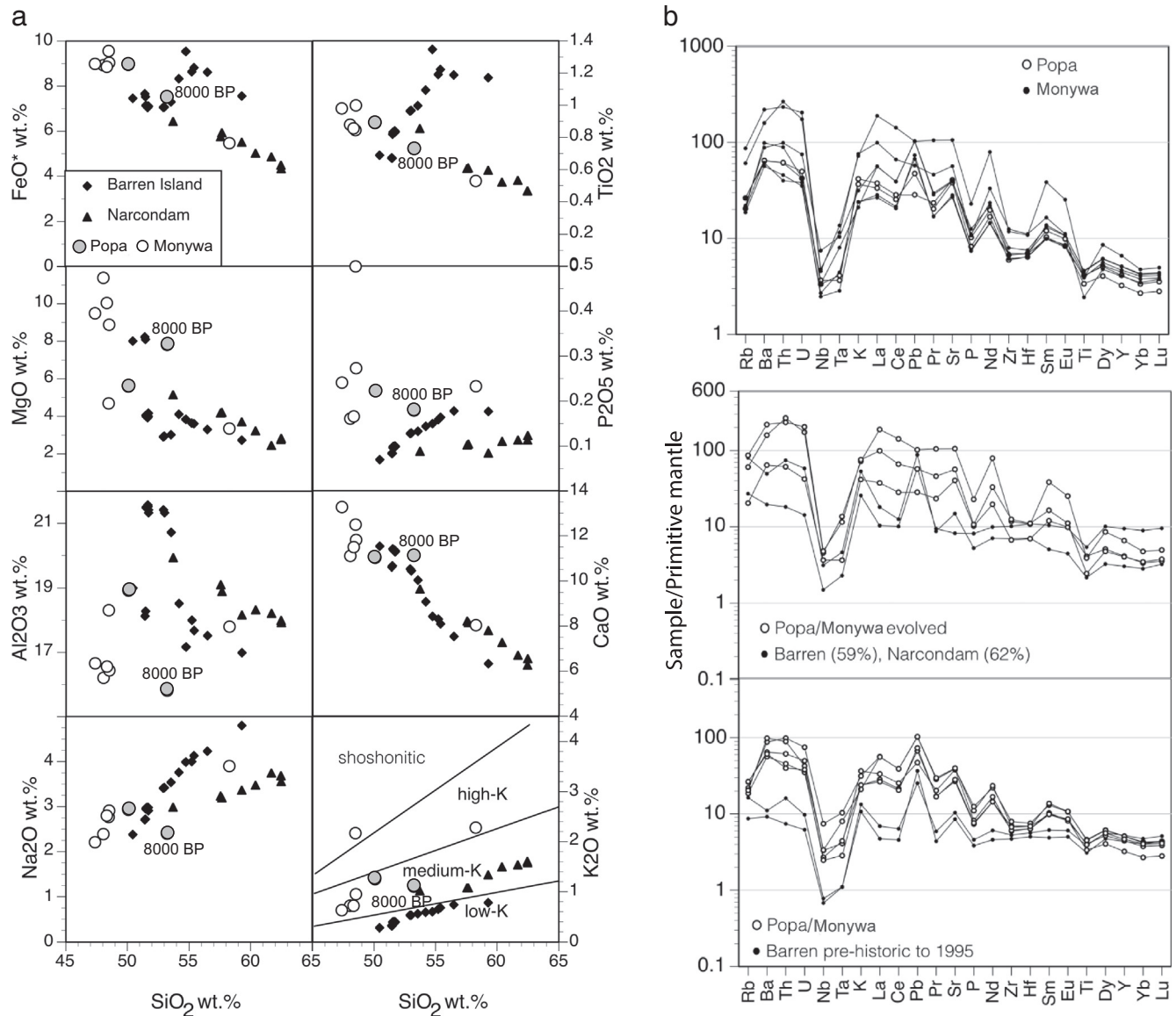
Fig. 7. Variations of major and trace elements concentrations in the samples of Mt. Popa, Monywa, Barren Island and Narcondam. (a) Harker diagrams. Composition of the 8000 BP eruption of Mt. Popa is highlighted. (b) Multi-element diagram. Evolved means low MgO, high SiO_2 or low Cr and Ni.

the edifice). Rapid unloading of the lithostatic pressure from the rising magma batch intensified the forthcoming eruption, and it occurred in the form of rather significant (~0.1 km^3) pyroclastic flow ("Shiveluch scenario" of the collapse-related eruptions of Belousov et al., 2007).

The edifice collapse and the emplacement of the pyroclastic flow were the last eruptive events we found in the geological record of Mt. Popa. Thick soil covering the deposits of the volcaniclastic fan does not contain ash layers. Thus, there were no substantial explosive eruptions of the volcano since ~8000 BP. The event 442 BCE mentioned in the local legend and interpreted by Chhibber (1934) as volcanic eruption was either of very small scale that left no signs in the geological record, or was just the tectonic earthquake without the accompanying eruptive activity. Bell (1907), who first reported about the legend, wrote "According to tradition there was a great earthquake in 442 B.C., during which the great cone of Popa rose from the plains: but the native chroniclers leave no record of how long it was active and when it became extinct." The described rising of Mt. Popa is obviously a fantastic phenomenon that can't be unequivocally interpreted as volcanic eruption.

6.2. Magmas of the Burma arc

The most recent eruption of Mt. Popa ~8000 BP produced basaltic andesite that is geochemically similar to the earlier products of the volcano as well as to the products of the Pliocene-recent eruptions of Monywa area. Comparing samples of these two subduction-related on-land volcanoes of Burma arc to the two oceanic counterparts, Barren Island and Narcondam volcanoes of the Andaman Sea (e.g. Streck et al., 2011), the following observations can be made: Nearly all basalt samples from Popa and Monywa are at the high end of Ca, Fe, Mg, Ti and P and most have considerable lower Al concentrations than Barren Island and Narcondam (Fig. 7a). Popa and Monywa samples tend to be much more enriched in incompatible trace elements and basaltic samples have steeper REE patterns than basaltic samples of Barren Island and Narcondam volcanoes. All, however, share low U/Th (0.12–0.24) and high Th/Nb (1.6–7) with Barren Island and Narcondam samples (cf., Fig. 11.12 of Streck et al., 2011). These low and high ratios appear to be characteristics for this arc when compared to global island arc data of Elliott (2003). In fact based on these ratios, Popa, Monywa, Narcondam and Barren Island define an end-member in this global
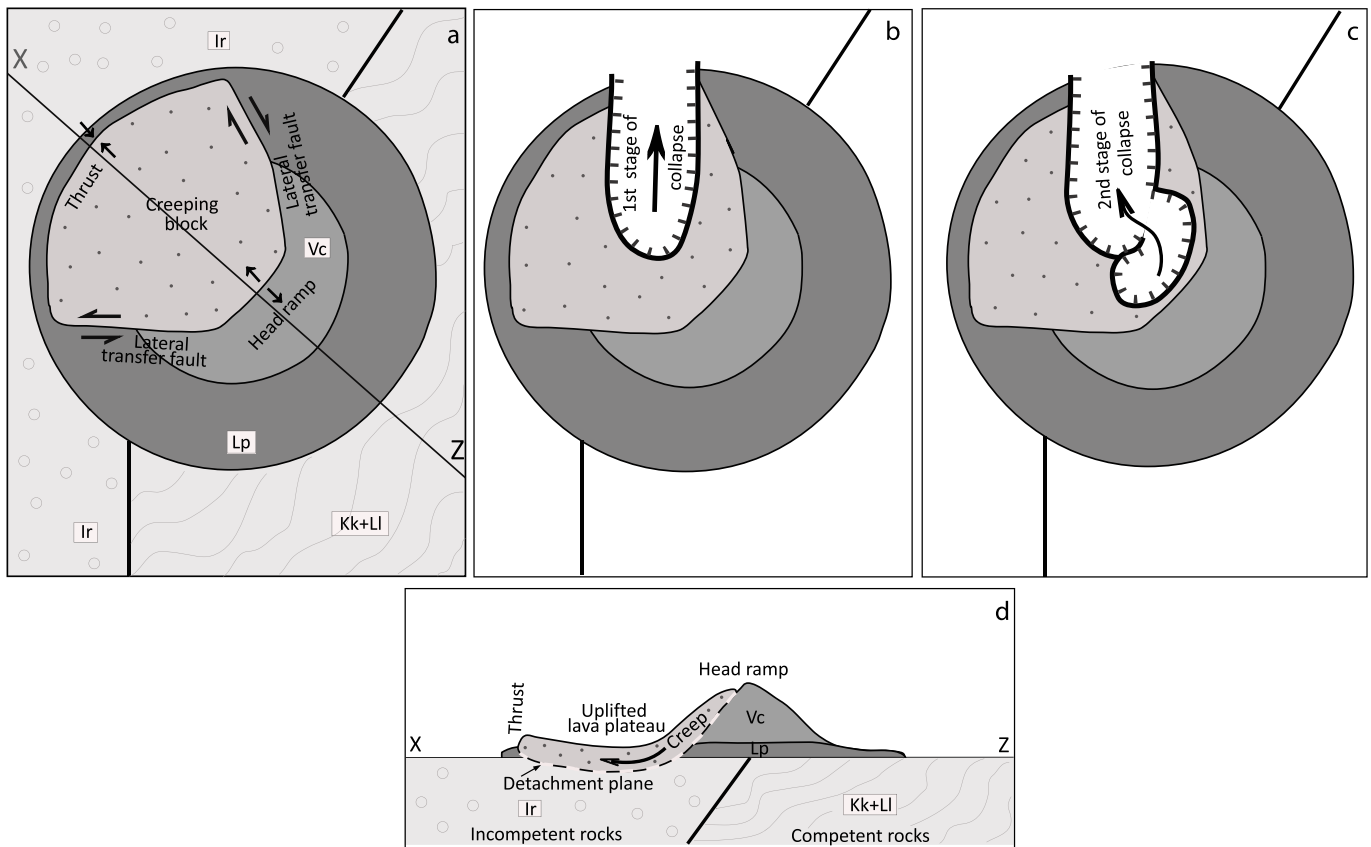
Fig. 8. Sketch showing development of asymmetric gravitational spreading and lateral collapse of the edifice of Mt. Popa. Upper pictures - plan view; lower picture - cross section. (a) Initiation of lateral gravitational creep and formation of listric fault. (b) First stage of collapse (c) Second stage of collapse. (d) Cross section along the line X–Z. See Fig. 2 for the indexes of geological formations (for simplification geological formations are not shown in b, c, and in the creeping block).

data set. The strong depletion of Nb and Ta and Ti is a feature of samples from all these four volcanoes. On the other hand, the depletion of the other high-field strength elements, Zr and Hf, observed in Popa and Monywa samples, is not seen in Narcondam or Barren Island samples and thus suggest that this depletion may be a function of whether a volcano is located on continental or oceanic crust. Similarly, greater enrichment in highly incompatible trace elements including LREE enrichment but low Rb in Monywa and Popa could be explained by a stronger influence of a metasomatized lithospheric mantle beneath continental crust.

6.3. Past and future eruptions in Myanmar

Our data confirmed the calc-alkaline geochemistry and subduction-related origin of the Pliocene-recent volcanoes of Burma arc outlined by previous researchers (e.g. Maury et al., 2004; Mitchell et al., 2012). There are comprehensive geodetic and seismological evidences of ongoing subduction in Myanmar (e.g. Socquet et al., 2006; Hurukawa et al., 2012). The subduction is highly oblique and very slow (13 mm/year of convergence), producing sparsely distributed volcanoes with low magma production rate (Mt. Popa 3×10^{-5} km^3/year) and rare eruptions that is common for such tectonic environment (Sample and Karig, 1982; Wadge, 1984). Thus, the repose period lasting 8000 years after the last eruption of Mt. Popa should not lead to conclusion that this volcano is extinct. It is widely accepted, e.g. by the Smithsonian Global Volcanism Program, that a volcano can be considered active if it has erupted within the past 10,000 years (Szakács, 1994). Some volcanoes of the Sunda arc demonstrated even longer periods of dormancy. For example, Gede volcano in Java has the same magma production rate as Mt. Popa and resumed its activity after the repose period that lasted >30,000 years (Belousov et al., 2015). Because of the above considerations Mt. Popa should be listed as active volcano.

Apart from the polygenetic volcano of Mt. Popa, the Burma volcanic arc has well-preserved monogenetic volcanoes in the Monywa area, where recent volcanism continues since Pliocene. The well-preserved NE trending chain of at least 5 maars includes the Twinywa maar that was formed 85 ± 12 ka BP (Ar/Ar age). This is the youngest age obtained for volcanic products of the Monywa area up to date. Other maars of the chain have not been dated yet and some of them may have been formed in Holocene. This area, along with Mt. Popa, has potential for future eruptions.

Sluggish modern volcanism in Myanmar associated with highly oblique subduction is not unique. Similar tectonic regimes exist, for example, in westernmost parts of Aleutian and Ryukyu arcs (Newberry et al., 1986; Lin et al., 2014). These areas also have widely scattered volcanoes with no historical eruptions. However, geological and seismological evidences has been recently obtained, suggest that submarine Piip volcano in western Aleutians as well as Tatun volcanic group in northern Taiwan are active (Yogodzinski et al., 1994; Belousov et al., 2010; Zellmer et al., 2015). Tatun volcano last erupted about 6000 years ago and underlain by a chamber of molten magma at a depth 30 km (Lin, 2016).

7. Conclusions

1. The latest period of volcanic activity of Mount Popa took place in the beginning of Holocene. It included several mild explosive eruptions of vulcanian type in the period from 12,700 to 8500 BP, as well as approximately 8000 BP the gravitational edifice collapse with the volume of 1.3 km^3 that was followed by VEI 3 magmatic eruption with deposition of 0.1 km^3 of pyroclastic flow of calc-alkaline basaltic andesite composition. Mt. Popa should be listed as active volcano.

2. The 8000 BP edifice collapse of Mt. Popa was preceded by long-term gravitational spreading (creep) of the volcanic cone. The spreading was highly asymmetric because NW part of the volcano base was built over mechanically weak sandstones of Irrawaddy Formation. The listric fault, which was formed during the creep, determined the direction of the collapse and complex morphology of the resulted crater.

3. Holocene eruptions of calc-alkaline composition in the Burma volcanic arc represent volcanological evidence of the ongoing subduction on the Arakan Trench. The low magma production rate of Mt. Popa (3×10^{-5} km^3/year averaged for the 1 Ma of the volcano history) is in agreement with the highly oblique angle and slow rate of the subduction.

4. Mt. Popa and monogenetic volcanic field of Monywa deserve detailed volcanological and sesmological studies.

Supplementary data to this article can be found online at https://doi.org/10.1016/j.jvolgeores.2018.06.010.

Acknowledgements

References

Bell, E.N., 1907. A Monograph on Iron and Steel Work in Burma. Superintendent, Government Printing, Rangoon, Burma (31 pp.).

Belousov, A., Belousova, M., Voight, B., 1999. Multiple edifice failures, debris avalanches and associated eruptions in the Holocene history of Shiveluch volcano, Kamchatka, Russia. Bull. Volcanol. 61, 324–342.

Belousov, A., Voight, B., Belousova, M., 2007. Directed blasts and blast-currents: a comparison of the Bezymianny 1956, Mount St Helens 1980, and Soufriere Hills, Montserrat 1997 eruptions and deposits. Bull. Volcanol. 69, 701–740.

Belousov, A., Belousova, M., Chen, C.-H., Zellmer, G., 2010. Deposits, character and timing of recent eruptions and gravitational collapses in Tatun Volcanic Group, Northern Taiwan: hazard-related issues. J. Volcanol. Geotherm. Res. 191, 205–221.

Belousov, A., Belousova, M., Krimer, D., Costa, F., Prambada, O., Zaennudin, A., 2015. Volcaniclastic stratigraphy of Gede Volcano, West Java, Indonesia: how it erupted and when. J. Volcanol. Geotherm. Res. 301, 238–252.

Bender, F., 1983. Geology of Burma. Gebrüder Borntraeger, Berlin (293 pp.).

Bertrand, G., Rangin, C., 2003. Tectonics of the western margin of the Shan plateau (central Myanmar): implication for the India–Indochina oblique convergence since the Oligocene. J. Asian Earth Sci. 21, 1139–1157.

Boyer, S.E., Elliott, D., 1982. Thrust systems. AAPG Bull. 66 (9), 1196–1230.

Cherkinsky, A., Wallace, K., 2017. Radiocarbon age of soil organic matter fractions buried by tephra in Alaska. Radiocarbon 59 (2), 465–472.

Chhibber, H.L., 1934. Geology of Burma. McMillan, London (538 pp.).

Clarke, A., Ongaro, T.E., Belousov, A., 2015. Vulcanian explosions. In: Sigurdsson, H., et al. (Eds.), The Encyclopedia of Volcanoes. Elsevier, pp. 505–518.

Crisp, J.A., 1984. Rates of magma emplacement and volcanic output. J. Volcanol. Geotherm. Res. 20, 177–211.

Cumming, G.V., Chitko, S., Tun, Soe Thura, Oo, Zaw Naing, Khin, Zaw, Than Myint, U., 2007. Lithofacies Associations and Eruptive History of Mount Popa: A Composite Cone Volcano in Central Myanmar. Asia Oceania Geological Society (AOGS), Bangkok, Thailand.

Curray, J.R., 1989. The Sunda Arc: a model for oblique plate convergence. Neth. J. Sea Res. 24 (2–3), 131–140.

Dasgupta, S., Mukhopadhyay, M., Bhattacharya, A., Jana, T.K., 2003. The geometry of the Burmese-Andaman subducting lithosphere. J. Seismol. 7, 155–174.

De Vries, B.V.W., Francis, P.W., 1997. Catastrophic collapse at stratovolcanoes induced by gradual volcano spreading. Nature 387, 387–390.

Delcamp, A., De Vries, B., James, M.R., 2008. The influence of edifice slope and substrata on volcano spreading. J. Volcanol. Geotherm. Res. 177, 925–943.

DeMets, C., Gordon, R.G., Argus, D.F., Stein, S., 1990. Current plate motions. Geophys. J. Int. 101, 425–478.

Elliott, T., 2003. Tracers of the slab. Inside the subduction factory. Geophys. Monogr. 138, 23–45.

Glicken, H., 1996. Rockslide-debris avalanche of May 18, 1980, Mount St. Helens Volcano, Washington. US Geological Survey, Open-file Report (No. 96-677).

Hurukawa, N., Pa Pa Tun, P., Shibazaki, B., 2012. Detailed geometry of the subducting Indian Plate beneath the Burma Plate and subcrustal seismicity in the Burma Plate derived from joint hypocenter relocation. Earth Planets Space 64, 333–343.

Lee, H.Y., Chung, S.L., Yang, H.M., 2016. Late Cenozoic volcanism in central Myanmar: geochemical characteristics and geodynamic significance. Lithos 245, 174–190.

Lin, C.H., 2016. Evidence for a magma reservoir beneath the Taipei metropolis of Taiwan from both S-wave shadows and P-wave delays. Nat. Sci. Rep. 6, 39500.

Lin, J.Y., Sibuet, J.C., Hsu, S.K., Wu, W.N., 2014. Could a Sumatra-like megathrust earthquake occur in the south Ryukyu subduction zone? Earth Planets Space 66, 49.

Maury, R.C., Pubellier, M., Rangin, C., Wulput, L., Cotten, J., Socquet, A., Belon, H., Juillaud, J.-P., Htun, H.M., 2004. Quaternary calc-alkaline and alkaline volcanism in an hyper-oblique convergence setting, central Myanmar and western Yunnan. Bull. Soc. Geol. Fr. 175 (5), 461–472.

Mitchell, A.H.G., Chung, S.L., Oo, Thura, Lin, T.H., Hung, C.H., 2012. Zircon U–Pb ages in Myanmar: magmatic–metamorphic events and the closure of a neo-Tethys ocean? J. Asian Earth Sci. 56, 1–23.

Newberry, J.T., Laclair, D.L., Fujita, K., 1986. Seismicity and tectonics of the far western Aleutian Islands. J. Geodyn. 6 (1–4), 13–32.

Newhall, C.G., Self, S., 1982. The volcanic explosivity index (VEI) an estimate of explosive magnitude for historical volcanism. J. Geophys. Res. Oceans Atmos. 87 (C2), 1231–1238.

Pivnik, D.A., Nahm, J., Tucker, R.S., Smith, G.O., Nyein, Kyaw, Nyunt, Maung, Maung, Hla, 1998. Polyphase deformation in a fore-arc/back-arc basin, Salin subbasin, Myanmar (Burma). AAPG Bull. 82 (10), 1837–1856.

Reiche, P., 1937. The Toreva-Block: a distinctive landslide type. J. Geol. 538–548.

Sample, J.C., Karig, D.E., 1982. A volcanic production rate for the Mariana Island arc. J. Volcanol. Geotherm. Res. 13, 73–83.

Satyabala, S.P., 1998. Subduction in the Indo-Burma Region: is it still active? Geophys. Res. Lett. 25 (16), 3189–3192.

Satyabala, S.P., 2003. Oblique plate convergence in the Indo-Burma (Myanmar) subduction region. Pure Appl. Geophys. 160 (9), 1611–1650.

Scharpenseel, H.W., Schiffmann, H., 1977. Radiocarbon dating of soils, a review. J. Plant Nutr. Soil Sci. 140 (2), 159–174.

Sheth, H.C., Ray, J.S., Bhutani, R., Kumar, A., Smitha, R.S., 2009. Volcanology and eruptive styles of Barren Island: an active mafic stratovolcano in the Andaman Sea, NE Indian Ocean. Bull. Volcanol. 71 (9), 1021.

Siebert, L., 1984. Large volcanic debris avalanches: characteristics of source areas, deposits, and associated eruptions. J. Volcanol. Geotherm. Res. 22, 163–197.

Socquet, A., Vigny, C., Chamot-Rooke, N., Simons, W., Rangin, C., Ambrosius, B., 2006. India and Sunda plates motion and deformation along their boundary in Myanmar determined by GPS. J. Geophys. Res. Solid Earth 111, B05406.

Steckler, M.S., Akhter, S.H., Seeber, L., 2008. Collision of the Ganges–Brahmaputra Delta with the Burma Arc: implications for earthquake hazard. Earth Planet. Sci. Lett. 273, 367–378.

Stephenson, D., Marshall, T.R., 1984. The petrology and mineralogy of Mt. Popa Volcano and the nature of the late-Cenozoic Burma Volcanic Arc. J. Geol. Soc. 141 (4), 747–762.

Stephenson, D., Reading, H., 1979. Discussion on magmatism and tectonics in SE Asia. J. Geol. Soc. 136, 587.

Streck, M.J., Ramos, F., Gillam, A., Haldar, D., Duncan, R.A., 2011. The intra-oceanic Barren Island and Narcondam arc volcanoes, Andaman Sea: implications for subduction inputs and crustal overprint of a depleted mantle source. Topics in Igneous Petrology. Springer, Netherlands, pp. 241–273.

Szakács, A., 1994. Redefining active volcanoes: a discussion. Bull. Volcanol. 56 (5), 321–325.

Szakács, A., Krézsek, C., 2006. Volcano–basement interaction in the Eastern Carpathians: explaining unusual tectonic features in the Eastern Transylvanian Basin, Romania. J. Volcanol. Geotherm. Res. 158 (1–2), 6–20.

Tregoning, P., Brunner, F.K., Bock, Y., Puntodewo, S.S.O., McCaffrey, R., Genrich, J.F., Calais, E., Rais, J., Subarya, C., 1994. First geodetic measurement of convergence across the Java Trench. Geophys. Res. Lett. 21, 2135–2138.

Wadge, G., 1984. Steady state volcanism: evidence from eruption histories of polygenetic volcanoes. J. Geophys. Res. Solid Earth 87 (B5), 4035–4049.

Walker, G.P., 1971. Grain-size characteristics of pyroclastic deposits. J. Geol. 79 (6), 696–714.

Wang, Y., Amundson, R., Trumbore, S., 1996. Radiocarbon dating of soil organic matter. Quat. Res. 45 (3), 282–288.

Yogodzinski, G.M., Volynets, O.N., Koloskov, A.V., Seliverstov, N.I., Matvenkov, V.V., 1994. Magnesian andesites and the subduction component in a strongly calc-alkaline series at Piip Volcano, Far Western Aleutians. J. Petrol. 35, 163–204.

Zellmer, G.F., Rubin, K.H., Miller, C.A., Shellnutt, J.G., Belousov, A., Belousova, M., 2015. Resolving discordant U–Th–Ra ages: constraints on petrogenetic processes of recent effusive eruptions at Tatun Volcano Group, northern Taiwan. Geol. Soc. Spec. Publ. 422, 175–188.